Opto-Electronic Science

Article

October 2023, Vol. 2, No. 10

DOI: 10.29026/oes.2023.230016

Light-stimulated adaptive artificial synapse based on nanocrystalline metal-oxide film

Igor S. Balashov[1], Alexander A. Chezhegov[1], Artem S. Chizhov[2], Andrey A. Grunin[1], Konstantin V. Anokhin[3,4] and Andrey A. Fedyanin[1]*

Artificial synapses utilizing spike signals are essential elements of new generation brain-inspired computers. In this paper, we realize light-stimulated adaptive artificial synapse based on nanocrystalline zinc oxide film. The artificial synapse photoconductivity shows spike-type signal response, long and short-term memory (LTM and STM), STM-to-LTM transition and paired-pulse facilitation. It is also retaining the memory of previous exposures and demonstrates spike-frequency adaptation properties. A way to implement neurons with synaptic depression, tonic excitation, and delayed accelerating types of response under the influence of repetitive light signals is discussed. The developed artificial synapse is able to become a key element of neuromorphic chips and neuromorphic sensorics systems.

Keywords: neuromorphic photonics; synaptic adaptation; spiking neuron; neuromorphic computing; optoelectronic synaptic devises; nanocrystalline metal-oxide film

Balashov IS, Chezhegov AA, Chizhov AS, Grunin AA, Anokhin KV et al. Light-stimulated adaptive artificial synapse based on nanocrystalline metal-oxide film. *Opto-Electron Sci* **2**, 230016 (2023).

Introduction

Swiftly emerging artificial intelligence approaches are driving the search for new architectural solutions and ways to realize computation. Traditional digital von Neumann architecture is significantly limited in processing speed and energy efficiency due to the separation of memory elements from the central processing unit[1–4]. This limitation is especially critical for artificial intelligence tasks requiring continuous memory access. The human brain has the best energy efficiency among existing intelligent systems. The embodiment even of a small fraction of its capabilities in information processing devices becomes a game-changing technology for artificial intelligence systems.

The high energy efficiency of the human brain is achieved to a large degree due to the spiking mode of information transmission as well as to the joint implementation of information integration and memory functions in the neuronal units. Spike signals combine the advantages of digital computing stability and high information capacity of analog signals. The use of spike coding has been successfully implemented in spiking neural networks (SNNs)[5,6], which are very attractive because of low power consumption and successful large amounts of data processing[7]. Prospects of the SNN-based neuromorphic approach for solving artificial intelligence problems have been demonstrated for CMOS chips such as TrueNorth[5], Loihi[8], and SpiNNaker[9]. SNNs mimic sig-

[1]Faculty of Physics, Lomonosov Moscow State University, Moscow 119991, Russia; [2]Faculty of Chemistry, Lomonosov Moscow State University, Moscow 119991, Russia; [3]Institute for Advanced Brain Studies, Lomonosov Moscow State University, Moscow 119991, Russia; [4]P. K. Anokhin Research Institute of Normal Physiology, Moscow 125315, Russia.

*Correspondence: AA Fedyanin, E-mail: fedyanin@nanolab.phys.msu.ru

Received: 22 June 2023; Accepted: 23 October 2023; Published online: 6 December 2023

nal transmission in biological neural networks representing information in the form of a spike sequence time series[10]. However, the existing SNNs are based on a limited number of properties of biological neurons and their connections. The challenge remains to develop a more biologically plausible multilayer neural network, that provides a significant boost in the speed of neuromorphic computations.

The usage of optical signals for the transmission of synaptic spikes between neurons has several advantages over electronics-only solutions. The optoelectronic approach reduces heat losses and is suitable for making a large number of network connections and transmitting spikes at higher rates. In addition, light-stimulated and photoconductive materials were implemented in constructing artificial neurons and several neuron-like properties were demonstrated using these materials. Artificial synapses based on inorganic perovskite quantum dots operating with spike signals possess short-term memory (STM), long-term memory (LTM), STM-to-LTM transition, and paired-pulse facilitation (PPF)[11–13]. Synaptic behavior of hybrid perovskite platelets also includes potentiation, depression[14], and activity-dependent plasticity[15].

A wide variety of materials are used for light-stimulated artificial synapses[16–19]. For example, a thin-film transistor-like synaptic device based on $CsPbBr_3$ perovskite quantum dots and amorphous indium gallium zinc oxide was explored for brain-inspired computing[20]. A synaptic transistor-based thin film of indium zinc oxide and hafnium oxide was also demonstrated[21]. Memory and plasticity properties have been shown in the light-stimulated organic field-effect transistors[22]. Multilayered semiconductor structures are also utilized as materials with neuromorphic properties induced by light stimulation[23,24]. These neuromorphic photoelectric structures show the effects of associative memory, “learning-experience ” behavior[25,26], learning-forgetting-relearning process[4], "AND" and "OR" light logic functions[25]. The neuromorphic properties of photoconductive structures are also used for image and symbol recognition, as shown in several computer simulations[10,27].

Implementation of basic neuromorphic properties such as STM and LTM requires a photovoltaic structure to have at least two channels for generating free charge carriers with different time constants. During light exposure, the conductivity of nanocrystalline metal-oxide films changes due to the generation of photoexcited electron-hole pairs and the adsorption and desorption of oxygen on the hierarchically ramified surface[28]. The difference in the rates of photoconductive processes in nanocrystalline metal oxide films makes them good candidate materials for neuromorphic synapses.

The memory of previous stimuli is one of the basic properties of the nervous system. Most neurons triggered by continuous stimulation initially respond with a high spike frequency followed by a firing rate decrease[29]. This important feature of neurodynamic behavior is called spike-frequency adaptation. Such adaptation function significantly expands the functionality of artificial neurons. A neuron with spike-frequency adaptation was recently implemented using, for example, an electrical neuromorphic circuit[30,31].

In this work, we propose an optical synaptic connection based on a nanocrystalline ZnO film. The photoconductivity of artificial ZnO-based synapse stimulated by the violet light pulses shows basic synaptic and neuronal properties including spike response, short- and long-term memory and paired-pulse facilitation. In addition, this structure displays the effect of memory about previous stimulations and spike-frequency adaptation. The presynaptic event affects both the photosensitivity and the dark photoconductivity decay of the artificial synapse. ZnO structures are low-cost and easy to manufacture and provide better photo- and environmental stability than, for example, perovskite halide materials, which is very important for long and reproducible neuron operation.

Results & discussion

Photoelectric synapse

The idea of a photoelectric synapse, which reproduces properties of biological synaptic transmission is shown in Fig. 1. In the nervous system, spike of presynaptic neuron leads to release of neurotransmitter transferred through the synaptic cleft to the membrane of the post-synaptic neuron where it activates its receptors and causes opening of the ion channels. As a result, the membrane conductivity changes and the excitatory post-synaptic current (EPSC) is generated[32]. Artificial synapse structure that embeds neural-like properties is shown in Fig. 1(a). Transmission of action potential is implemented optically through radiation of a LED light source that increases the conductivity of the semiconductor nanocrystalline ZnO film. When the light is turned off, the conductivity decreases over time. The form of light-

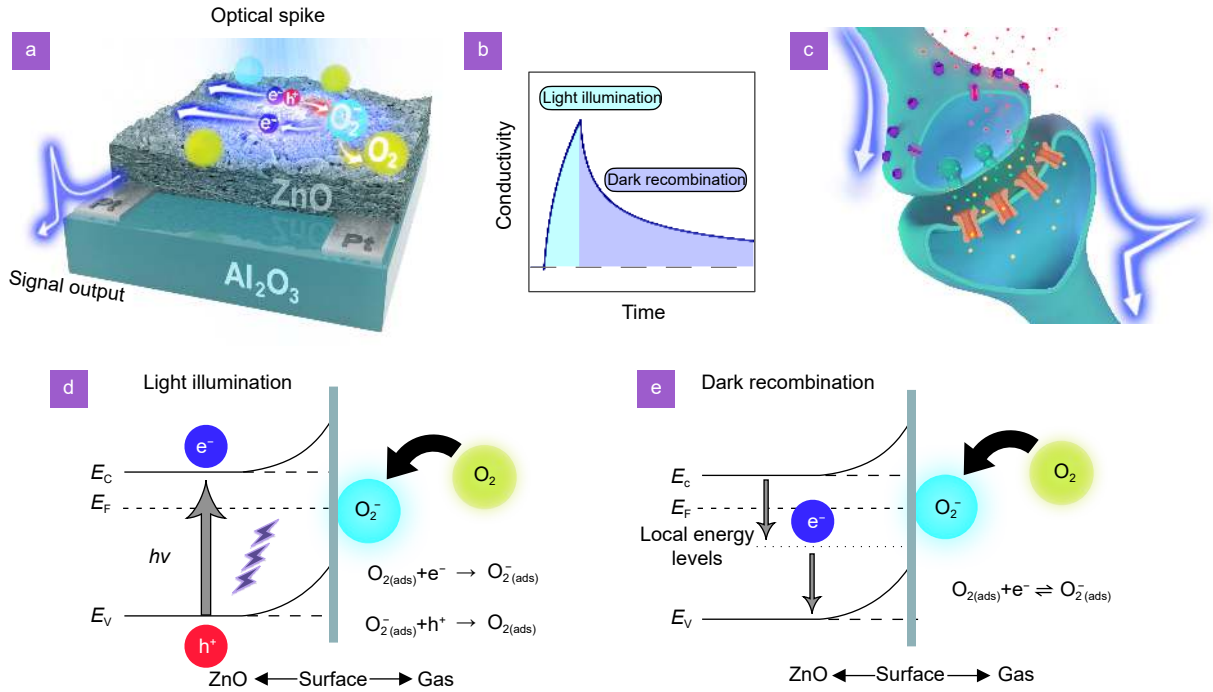

Fig. 1 | (**a**) 3D schematic illustration of light-stimulated artificial synapse based on nanocrystalline ZnO film. (**b**) Postsynaptic conductivity modulation induced by light. (**c**) 3D schematic illustration of a biological synapse. (**d**, **e**) Energy level diagrams of an optoelectronic synapse for light stimulation and dark electrons recombination.

induced change of postsynaptic conductivity resembles the shape of biological spikes.

Figure 1(b) shows a typical photoresponse of a nanocrystalline ZnO film irradiated with a single light pulse. Since the photoconductivity is a relaxation process, it has rise and decay kinetics resulting in a spike-like signal response to a square-shape light pulse. ZnO film is characterized by short rise time and much longer decay time. The electrical conductivity σ of nanocrystalline zinc oxide is controlled by potential barriers arising at the grain boundaries due to the chemisorption of oxygen molecules and exponentially depends on its height V_{surf}, $\sigma=\sigma_0\exp(-eV_{surf}/kT)$.

Light absorption by zinc oxide leads to generation of photoexcited charge carriers and an increase of photoconductivity due to delocalized electrons. At the same time, photoexcited electrons $e^-(h\nu)$ and holes $h^+(h\nu)$ interact with adsorbed oxygen species causing photoadsorption (1) and photodesorption (2)[33,34].

$$O_2(\text{ads}) + e^-(h\nu) = O_2^-(\text{ads}) \,, \qquad (1)$$

$$O_2^-(\text{ads}) + h^+(h\nu) = O_2(\text{ads}) \,, \qquad (2)$$

where O_2(ads) is a physically adsorbed oxygen molecule. As a result, the height of the potential barriers on the grains' surface changes. Thus, the photoconductivity decay at short time intervals (<10^2 s) is caused by the recombination of photoexcited electrons at various types of intrinsic traps, while at long time intervals (>10^3 s) it is controlled by the recovery of the concentration of chemisorbed oxygen on the grain surface and height of potential barriers to a "dark" value.

Characterization of photoconductive ZnO-based structures

The synthesized nanocrystalline ZnO has a wurtzite structure (Fig. 2(a)) with a specific surface area of 42±5 m^2/g. The average size of ZnO nanocrystallites calculated from the broadening of X-ray reflections is 11±1 nm. A detailed study of the size and the microstructure of ZnO crystallites by the HAADF-STEM method of a similar sample was published earlier[33]. Nanocrystalline zinc oxide has an optical absorption edge near 385 nm; the band gap calculated from the spectrum is 3.18 eV, see Fig. 2(b). The X-ray photoelectron spectra of the sample show a Zn2p doublet with a single charge state and an O1s singlet with two charge states (Fig. 2(c) and 2(d)). The single charge state of zinc is attributed to its oxidation state 2+ (E_B=1022.0 eV for $Zn2p_{3/2}$), while O1s(I) relates to oxygen in the crystal lattice of zinc oxide (E_B=530.8 eV) and O1s(II) is attributed to chemisorbed oxygen molecules or belonging to hydroxyl groups on the surface of ZnO (E_B=532.3 eV).

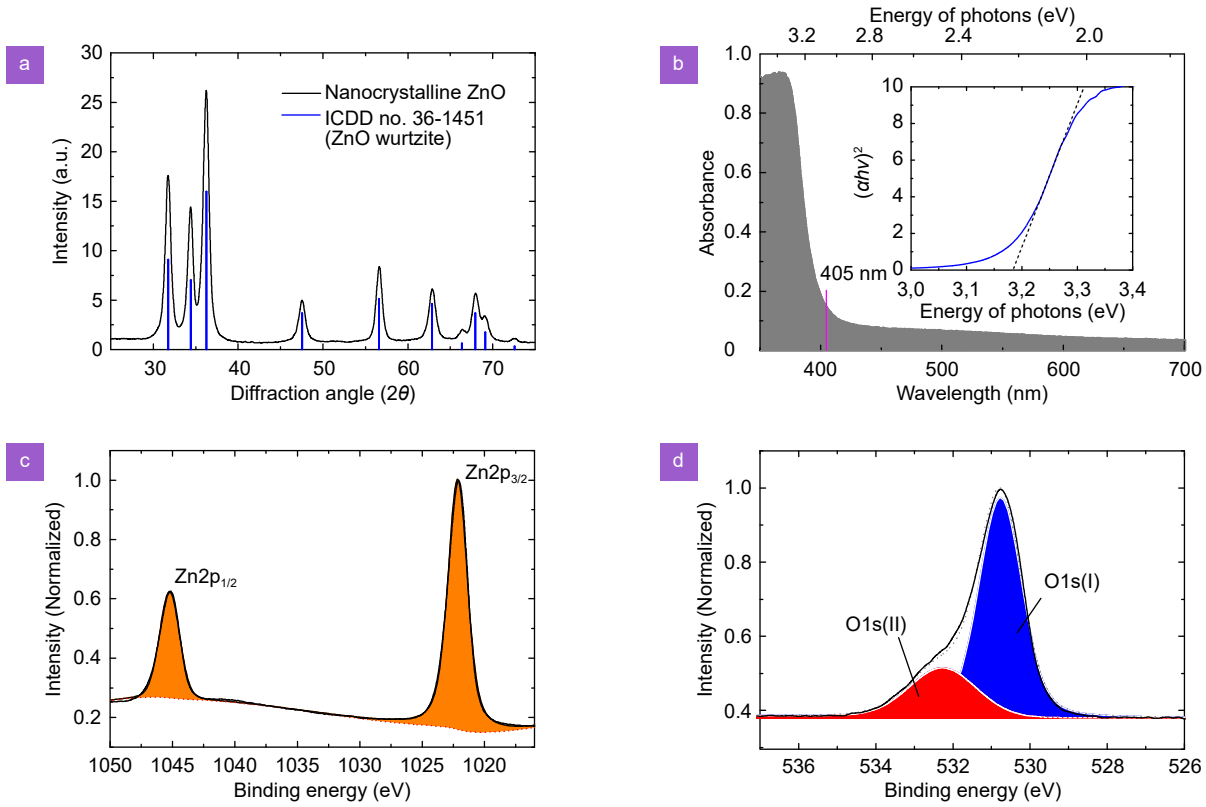

Fig. 2 | Nanocrystalline ZnO characterization. (**a**) X-ray diffraction pattern. (**b**) UV-vis absorbance spectrum, the inset is determination of E_g of nanocrystalline ZnO from optical absorption using a Tauc plot. (**c**,**d**) X-ray photoelectron spectra on the Zn2p (c) and O1s (d) regions.

Optical microscopy images of a device consisting of Al_2O_3 plate with Pt electrodes, as well as with an applied ZnO layer are shown in Fig. 3(a) and 3(b). Scanning electron microscopy of ZnO film showed its rough surface due to the formation of ZnO aggregates of various sizes. The film thickness estimated with a 70° tilt of the sample is approximately 50 μm, see Fig. 3(c). The average size of ZnO aggregates is in the range from 1 μm to 10 μm, although there are also larger and smaller particles, see Fig. 3(d). High-resolution SEM images show micrometer aggregates with porous structure molded from smaller aggregates from 50 nm to 100 nm in size, see Fig. 3(e). Thus, photoconductive ZnO films exhibit a hierarchical structure which is manifested itself in the appearance of primary aggregates of nanocrystalline ZnO, and then in the formation of secondary aggregates of micrometer scale. The presence of primary aggregates is also confirmed by the estimation of the average particle size from the specific surface area. Calculated at S_{spec}=42 m²/g and ρ=5.61 g/cm³, it leads to an average value of d_{BET}=25 nm in the spherical approximation.

Basic neuromorphic properties

Neuron-like response is demonstrated by illumination of the sample with a sequence of four pre-synaptic pulses with central wavelength of 405 nm, average intensity of 3.2 mW/cm², duration of 25 seconds and a 50% duty cycle (see Fig. 4(a)). When the LED is turned on, the structure shows an increase of conductivity. This leads to a rapid increase in EPSC corresponding to activity-dependent synaptic plasticity. When the LED is turned off, a gradually relaxing memory effect is observed. This process is the same as the EPSC decay in biological prototypes. As a result of electron-hole pairs recombination the conductivity decays to its initial value.

Light and dark photoconductivity switching in nanocrystalline ZnO is studied by applying two hours of light illumination (gray dashed line in Fig. 5(a)). Light-induced photoconductivity increases nonlinearly in time.

Figure 4(b) illustrates the decay of photoconductivity after 1200-second light illumination. The decay curve indicates free charge carriers decrease in time and is characterized by more than 8 hours of total relaxation time. The photoconductivity decrease arises due to two effects: oxygen molecules adsorption and recombination of nonequilibrium charge carriers inside crystals and on their surface. In dark conditions, the process of equilibrium surface oxygen concentration recovery occurs

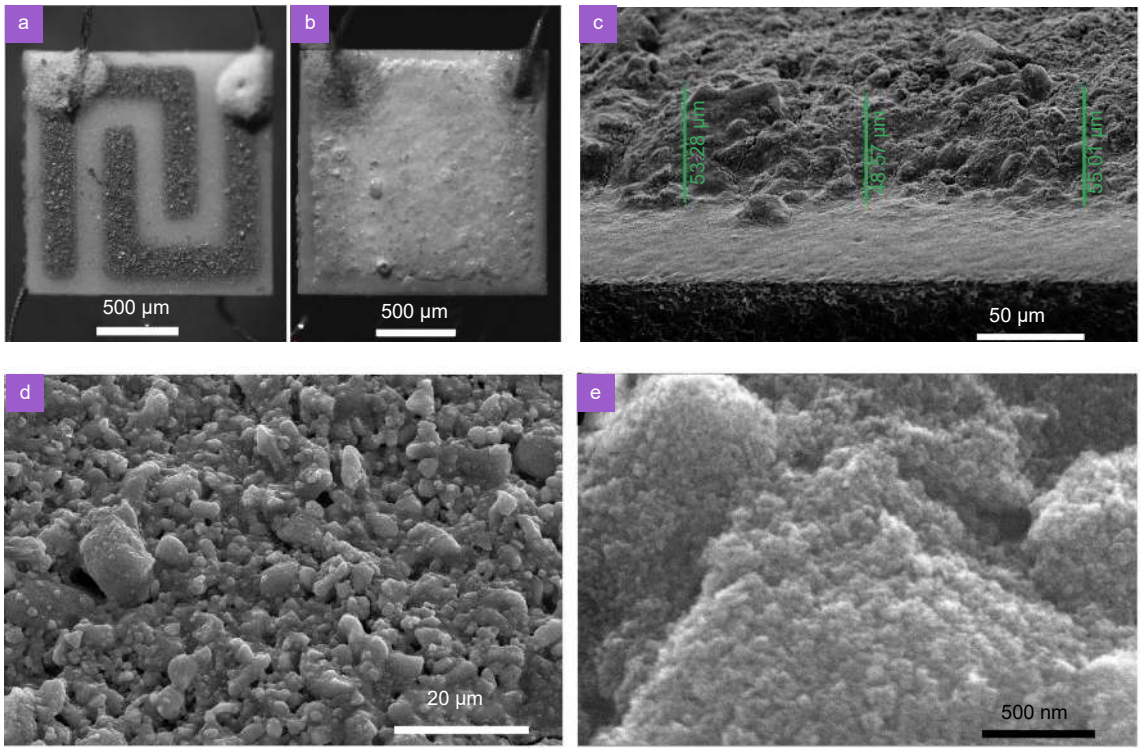

Fig. 3 | (**a**) Optical microscopy images of Al_2O_3 substrate with Pt electrodes and (**b**) covered with ZnO layer. Scanning electron microscopy images: (**c**) the edge of ZnO layer obtained as the sample is tilted by 70° to measure its thickness; (**d**) the ZnO layer surface; (**e**) individual aggregates forming a ZnO layer.

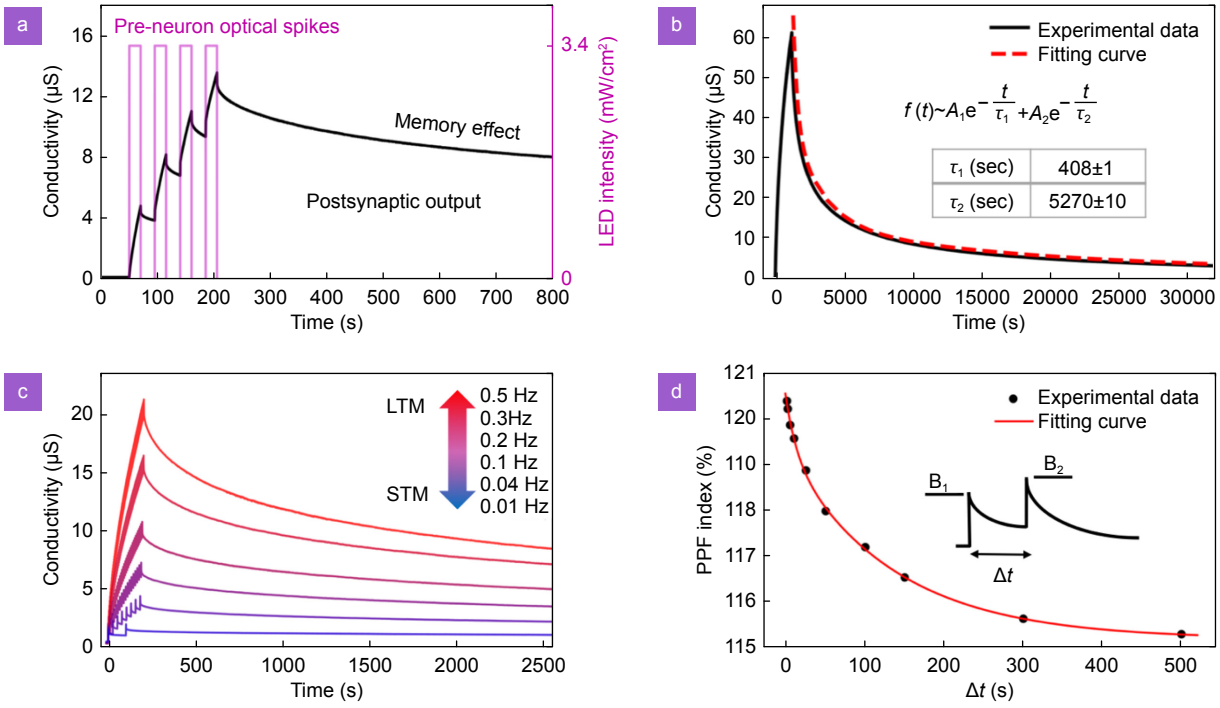

Fig. 4 | Basic neuromorphic photoelectric properties. (**a**) Postsynaptic conductivity (black curve) for four pre-synaptic light pulses lasting 25 seconds with 50% duty cycle (purple). (**b**) Postsynaptic conductivity after 1200 seconds light exposure and dark conductivity decay approximation. (**c**) STM-to-LTM transition emerging by frequency increase. (**d**) PPF index defined as the ratio of the amplitude B1 of the response to the first light pulse the amplitude B2 corresponding to the second spike plotted as a function of time delay between two spikes.

resulting in the decrease of semiconductors free charge carrier's concentration and electrical conductivity according to Eq. (1). The decay rates differ significantly for both effects. Initially, there is a rapid drop of conductivity due to the reverse internal photoelectric effect. Oxygen chemisorption at room temperature proceeds more slowly, which is due to the limited number of adsorption sites on the ZnO surface and an increase in the adsorption activation energy as free sites are filled. Taking into account the existence of two relaxation mechanisms, the photoconductivity decay is approximated as the sum of two decreasing exponentials:

$$\sigma(t) = A_0 + A_1 \exp\left(-\frac{t}{\tau_1}\right) + A_2 \exp\left(-\frac{t}{\tau_2}\right), \quad (3)$$

where adjustable parameters τ_1 and τ_2 have the meaning of the average charge carrier's lifetimes. The values of τ_1 = 408 s and τ_2 = 5270 s are chosen to fit a relaxation after 1200 seconds exposure.

The shape of conductivity relaxation line corresponds to the characteristics of biological synapse plasticity. Depending on the parameters of activation, synaptic plasticity is manifested at the short-term or long-term time scales[35]. STM reflects the aftereffects of presynaptic activity in the time range from milliseconds to minutes. LTM is long-term changes in synaptic strength lasting from tens of minutes to many hours, sometimes even days or months. Thus, temporal features of conductivity decay in nanocrystalline ZnO correspond to the plastic changes in biological synapses.

Transition of STM to LTM is the main mechanism of transformation of external stimulus into permanently stored information[36–38]. The nervous system is characterized by a memory consolidation phenomenon when STM is converted to LTM[39]. An optoelectronic synapse demonstrates STM-to-LTM transition at various frequencies of presynaptic spikes, see Fig. 4(c). The repetition rate of one-second light pulses was modulated from 0.01 Hz to 0.5 Hz. The decay rate of synaptic weights is frequency dependent, the higher the frequency of exposure the longer the decay of the synaptic weight value. STM-to-LTM transition occurs with increasing frequency. This behavior of the neuromorphic structures repeats the biological learning mechanisms[40].

PPF is one of the important properties of synaptic impulse transmission and occurs when a synapse is sequentially activated by two spikes with a short interval between them, and the second response is stronger than the first one. PPF is a form of short-term plasticity due to an increased neurotransmitter release in response to the second stimulation[41]. The magnitude of the response to the second spike depends on the time between paired pulses. Artificial synapse PPF is studied for 10 different interspike intervals in the range from 1 s to 500 s for 1 s light pulses. Strong increase in PPF is found for all spike sequences. Facilitation is characterized by the PPF index, that is determined as the ratio of the maximum postsynaptic conductance change amplitude B1 as a response to the first light spike over the amplitude B2 corresponding to the second spike. PPF index dependence interspike intervals is shown in Fig. 4(d) and decays with increasing the time between light spikes. The dependence is approximated by the sum of two decreasing exponentials:

$$PPF_{\text{ratio}} = 1 + C_1 \exp\left(-\frac{\Delta t}{\tau_3}\right) + C_2 \exp\left(-\frac{\Delta t}{\tau_4}\right), \quad (4)$$

where Δt is the time interval between two spikes, τ_3 and τ_4 are relaxation times. The best fit to the data is obtained for synaptic plasticity time values of τ_3 = 14 s and τ_4 = 135 s. The decay times of PPF relaxation and photoconductivity depend on the received energy, however, the magnitude of the ratio of the fast and slow phases, τ_3/τ_4, is maintained.

Spike-frequency adaptation

Neural adaptation – time-dependent modulation of neural responses following sequential stimuli – plays an important role in the nervous system[42]. Gradual reduction of excitability of a neuron in response to repeated presynaptic action potentials is a basic form of adaptation mediated through plastic changes in the synapse and is thought to underlie habituation – the simplest form of non-associative learning[43]. Implementation of adaptation properties in an artificial synapse leads to an emergence of a variety of forms of neuronal activity and plasticity phenomena[44,45].

In the experiment of the adaptation of a photoelectric synapse two levels of nanocrystalline conductivity are fixed. A semiconductor in the dark relaxed state is illuminated with continuous LED light until the upper selected conductivity value is reached. Then the LED source is turned off and the conduction value is recovered due to the relaxation processes. When the lower selected conductivity limit is reached, the LED radiation source is switched on again and the conductivity increases to the upper selected value. Such periodical LED on/off

switching with conductivity switching between two cutoff levels is carried out 100 times. This experiment makes it possible to study excitation and relaxation photoelectric synapse dynamics.

As noted above, the sample has a nonlinear conductivity growth upon the light illumination. This is used to choose adaptation patterns of artificial synapse. Four photoconductivity modulation ranges are selected with the 10 μS gap: 10 μS – 20 μS (Range 1), 30 μS – 40 μS (Range 2), 50 μS – 60 μS (Range 3), 70 μS – 80 μS (Range 4). The duration of relaxation and excitation for each of the 100 impulses is shown in Fig. 5(b) and 5(c). The synapse is less sensitive to the first pulses of presynaptic illumination. The transition time between the conductance levels during light illumination decays for each subsequent pulse. The relaxation time between specified conductivity levels also changes with each successive pulse. Rapid relaxation to the initial phase is replaced by the smooth increase in the relaxation time.

The drop of the conductivity inside the Range 4 requires longer presynaptic exposure time, but the change in exposure time turns out to be minor for all Ranges. Thus, the duration of the spikes with fixed conductivity gaps is similar for various ranges. However, the decay time varies significantly for different ranges. The fastest photoconductivity relaxation is observed for the Range 4, while the relaxation time for others is significantly larger. The duration of the interspike relaxation time with the fixed conductivity cutoff differs by two orders of magnitude for different conductivity ranges.

The adaptability of the artificial synapse frequency response is controlled by choosing the conduction cutoffs levels (see Fig. 6). Different adaptation patterns are achieved by choosing the range, e.g., an increase in frequency (red curve), a stable frequency (green curve) or a gradual decrease in frequency for each next spike (blue and orange curves).

The change in the duration of relaxation times within the measured ranges during pulsed illumination can be explained by the capture of photoexcited charge carriers in traps. Nanocrystalline ZnO contains various acceptor defects in its energy structure, such as vacancies and interstitial atoms, dangling bonds on the surface, and others[46,47]. The relaxation of photoexcited electrons from the conduction band of the ZnO occurs through their capture on acceptor traps, which form local levels within the band gap. This, in general, increases the lifetime of photoexcited charge carriers and greatly slows down the decay of photoconductivity.

With pulsed illumination, the first pulses lead only to partial filling of the traps with photoexcited electrons, and each subsequent pulse leads to the generation of electrons from a slightly different initial state than the

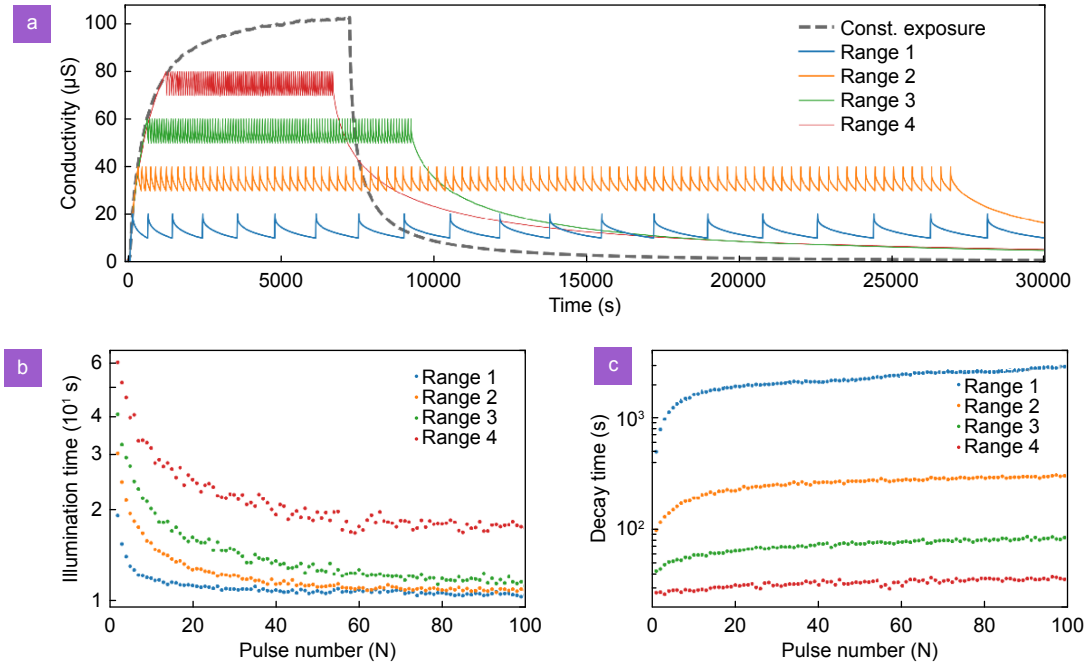

Fig. 5 | Adaptation studies. (**a**) 100 light-pulses sequential irradiation for four conductivity change ranges, 2-hour continuous illumination of ZnO-based synapse (gray dashed curve). (**b**) Logarithmic dependence of illumination duration for each of 100 pulses. (**c**) Logarithmic dependence of the relaxation after each of 100 pulses.

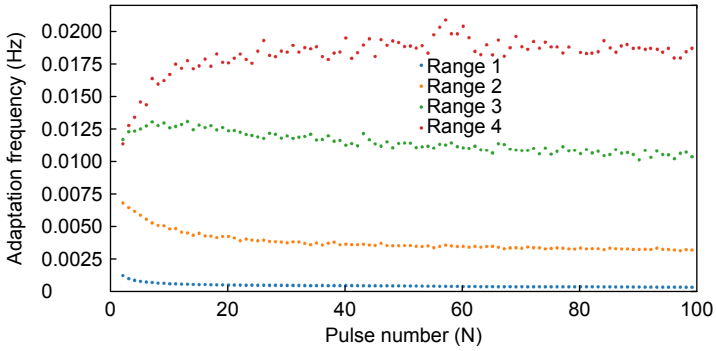

Fig. 6 | Spike frequency as a function of spike number for different conductivity change ranges.

previous one. Therefore, the times of illumination and decay of photoconductivity undergo changes within the selected ranges. Over time, a steady state is established between the processes of generation and recombination of charge carriers, which corresponds to constant intervals of illumination and decay of photoconductivity. The rate at which a steady state reached is proportional to the illumination time, which allows the trap levels to be filled faster with persistent illumination. It can be seen from the Fig. 5(a) that for the Range 4, reaching the level of 70–80 mS requires an initial exposure for a long time, while the Range 1 (10–20 mS) requires much shorter exposure time. Therefore, the time to reach the steady state for the Range 4 is expectedly less than for the Range 1.

Steps towards photoelectric neuron with adaptation

The search for biological analogies is one of the most promising approaches in the development of artificial intelligence, considering that properties of the nervous system can be emulated using photoelectric synapse. Adaptation empowers the neuron with a function of non-associative learning that is able to result in complex patterns of neuronal firing. The biological neuron executes various spike modes demonstrating tonic, adapting and delayed accelerating types of excitations[48]. These modes are realized in the studied photoelectric artificial synapse and shown in Fig. 6. Adaptive spikes whose frequency decreases in time are shown by blue and orange curves, tonic spiking is shown by green dots corresponding to an almost constant frequency generation and delayed accelerating spike mode is illustrated by red dot curves. Switching between different modes of excitation is achieved by choosing the cutoff level. The variety of spike patterns is not limited to the three displayed cases. Searching for implementations of other spike patterns, such as burst mode[49], is the subject of the further research.

Integrate-and-fire mathematical models describe propagation of a stimulus in a biological neuron[49]; they encode spikes as events and depict the time of occurrence of the neuron's action potentials. Izhikevich[50] and Adaptive Exponential (AdExp)[51] are the examples of integrate-and-fire models that take into account properties of neuronal adaptation. An AdExp model contains two differential equations, the first one describes changes of membrane potential, and the second one accounts for adaptation. A variety of neuronal firing patterns including tonic, adapting, delayed accelerating and bursting spike sequences can be described using such equations. These mathematical models are useful for describing the adaptation properties of photoelectric synapses.

The response to a repetitive signal increases or decreases depending on the modes of synaptic excitation. Synapses with different adaptation modes can be combined to obtain a system with a complex synaptic weight behavior potentially applicable in neuromorphic sensing as an anomaly amplifier or discriminator. The properties of stimulus-specific adaptation are important for processing of various sensory stimuli such as sound, somatosensory, and visual signals[52–54] and can be used for anomaly detection and feature selection. Figure 7 shows the concept of using frequency adaptation properties to process auditory signals. Neurons are arranged according to the principle described in the spike-frequency adaptation experiment in Fig. 5. Continuous signal from a presynaptic neuron causes semiconductor conductivity changes between the specified cutoff levels. Four types of differentiated sound stimuli coming from presynaptic neurons are shown in Fig. 7: baby crying, sounds of dialogue, background music and street noise. Each type of stimulus arrives at a separate synapse with individually tuned adaptation properties. Repetitive spike activity caused by background music and street noise results in an adaptive type of spike excitation and synaptic

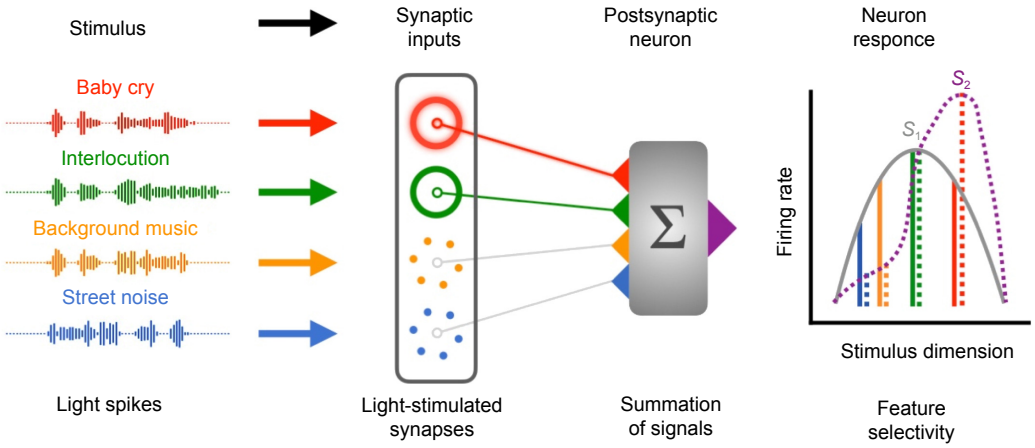

Fig. 7 | Integration of light-stimulated synapses with adaptation properties into computing platform. In the simplest way, the final artificial neuron firing rate is determined by its presynaptic inputs selectivity. The graph shows two types of response: S_1 corresponds to a neuron without synaptic inputs adaptation, S_2 is a response of a neuron with adaptation.

depression (gray curves). Tonic excitation synapse type configured to dialogue sounds does not reduce its responses. Due to this, the selectivity in the feature dimension shifts towards the perception of a dialog. Sound of a persisting baby crying causes delayed accelerating type of response, triggering an increase in postsynaptic potential. The postsynaptic response will shift the firing rate distribution towards the amplified feature. As a result, the specificity of the spiking rate response of a neuron is determined by adaptation mode adjustment of its synaptic inputs.

Experimental section

Synthesis and characterization of nanocrystalline ZnO films

Nanocrystalline ZnO was synthesized according to the method described earlier[55]. Precipitation of basic zinc carbonate from an aqueous solution by the reaction of $Zn(CH_3COO)_2$ with NH_4HCO_3 was used, $Zn_x(CO_3)_y(OH)_z$ was further decomposed at 300 °C in air. The nanocrystalline ZnO powder obtained after annealing was mixed with α-terpineol and the resulting suspension was applied to the surface of alumina plate equipped with Pt electrodes.

Phase composition and crystal structure of ZnO was studied by powder X-ray diffraction (XRD) with a Rigaku diffractometer using CuKα radiation with wavelength of λ=1.54059 Å (1 Å=10^{-10} m). The specific surface area of nanocrystalline ZnO was determined by the low-temperature nitrogen adsorption method. About of 100 mg of ZnO was placed in a test quartz tube and heated at 200 °C in a He flow for 1 h. Then the test tube with the sample was cooled to room temperature, placed in a dewar with liquid nitrogen, while a mixture of 10% N_2 in He was passed through the test tube. Using the Chemisorb 2750 (Micromeritics), the volume of adsorbed nitrogen was measured, and when the test tube was heated to room temperature, the volume of desorbed nitrogen was measured. Based on the obtained values, the surface area was determined using the Brunauer-Emmett-Teller (BET) model[56] which was related to the mass of the sample to obtain the specific surface area (m^2/g).

Absorption spectrum of nanocrystalline ZnO film in the wavelength range from 300 nm to 800 nm was recorded using Perkin–Elmer Lambda 35 spectrometer. X-ray photoelectron spectroscopy (XPS) measurements were performed using a K-Alpha (Thermo Scientific) spectrometer with an Al Kα X-ray source (E = 1486.7 eV). The charge correction was performed relative to the main carbon C1s peak, the binding energy of which was assumed to be 285 eV. The morphology of the photosensitive ZnO layer was studied by SEM using a Prisma E (Thermo Fisher Scientific). Before the measurements, a thin Au layer was sputtered on the sample. To evaluate the film thickness, the sample was tilted 70° relative to the horizontal. The scalability aspects of the synthesis methods, the technologization of the fabrication process, and the variability of synaptic cell parameters for different batches require a separated study.

Photoelectric synapse measurements

The conductivity measurements of the ZnO film were carried out with the voltage drop measurement circuit across a series-connected additional resistance (high-precision resistor 12 kΩ 0.05%) with subsequent calculation of the conductivity. A linear voltage regulator

(AMS1117-3.3) with an output voltage of 3.3 V and an output current of up to 80 mA was used as a reference source. The voltage across the additional resistance was measured using a 16-bits ADC converter (ADS1115). The sampling time step was 1 ms.

An LED with the central wavelength of 405 nm was used as an illumination source. It was mounted on the same axis with the structure at the distance of 20 mm, the light intensity at the film surface was 3.2 mW/cm^2. To reduce the influence of variable temperature and humidity of the environment an airtight black box was used.

Conclusions

A light-stimulated artificial synapse based on nanocrystalline ZnO film is proposed and implemented. It reproduces basic properties of neuronal synapses including the ability to transfer spike signals, short-term memory, long-term memory, and paired-pulse facilitation. ZnO film displays a synaptic-like response to presynaptic light stimulation. The synapse has a non-linear EPSC time dependence. PPF index is studied for different interspike intervals in the range between 1 s to 500 s for one second light pulses. An artificial synapse has two types of memory: STM lasting a few seconds and LTM maintained for an order of magnitude longer. An STM-to-LTM transition is shown at different frequencies of presynaptic stimulations. Conductivity properties of photoelectric synapse imitate the features of presynaptic action potential adaptation in natural neurons. Choosing the conductivity cutoff level one can control the adaptability to the frequency response. Proposed optoelectronic synapse has advantages over the previous digital neuron models with adaptation based on microelectronic components. The combination of these properties makes the nanocrystalline ZnO film-based synapse a promising element for bioinspired neuromorphic computation.

References

1. Ferreira de Lima T, Shastri BJ, Tait AN, Nahmias MA, Prucnal PR. Progress in neuromorphic photonics. *Nanophotonics* **6**, 577–599 (2017).
2. Lai DX, Li EL, Yan YJ, Liu YQ, Zhong JF et al. Gelatin-hydrogel based organic synaptic transistor. *Org Electron* **75**, 105409 (2019).
3. Mao JY, Zhou L, Zhu XJ, Zhou Y, Han ST. Photonic memristor for future computing: a perspective. *Adv Opt Mater* **7**, 1900766 (2019).
4. Ding GL, Yang BD, Zhou K, Zhang C, Wang YX et al. Synaptic plasticity and filtering emulated in metal–organic frameworks nanosheets based transistors. *Adv Electron Mater* **6**, 1900978 (2020).
5. Merolla PA, Arthur JV, Alvarez-Icaza R, Cassidy AS, Sawada J et al. A million spiking-neuron integrated circuit with a scalable communication network and interface. *Science* **345**, 668–673 (2014).
6. Yamazaki K, Vo-Ho VK, Bulsara D, Le N. Spiking neural networks and their applications: a review. *Brain Sci* **12**, 863 (2022).
7. Taherkhani A, Belatreche A, Li YH, Cosma G, Maguire LP et al. A review of learning in biologically plausible spiking neural networks. *Neural Netw* **122**, 253–272 (2020).
8. Davies M, Srinivasa N, Lin TH, Chinya G, Cao YQ et al. Loihi: a neuromorphic manycore processor with on-chip learning. *IEEE Micro* **38**, 82–99 (2018).
9. Furber SB, Galluppi F, Temple S, Plana LA. The spinnaker project. *Proc IEEE* **102**, 652–665 (2014).
10. Yin L, Han C, Zhang QT, Ni ZY, Zhao SY et al. Synaptic silicon-nanocrystal phototransistors for neuromorphic computing. *Nano Energy* **63**, 103859 (2019).
11. Wang K, Dai SL, Zhao YW, Wang Y, Liu C et al. Light - stimulated synaptic transistors fabricated by a facile solution process based on inorganic perovskite quantum dots and organic semiconductors. *Small* **15**, 1900010 (2019).
12. Wang Y, Lv ZY, Zhou L, Chen XL, Chen JR et al. Emerging perovskite materials for high density data storage and artificial synapses. *J Mater Chem C* **6**, 1600–1617 (2018).
13. Gupta GK, Kim IJ, Park Y, Kim MK, Lee JS. Inorganic perovskite quantum dot-mediated photonic multimodal synapse. *ACS Appl Mater Interfaces* **15**, 18055–18064 (2023).
14. Ge SP, Huang FC, He JQ, Xu ZS, Sun ZH et al. Bidirectional photoresponse in perovskite - ZnO heterostructure for fully optical-controlled artificial synapse. *Adv Opt Mater* **10**, 2200409 (2022).
15. Gong JD, Yu HY, Zhou X, Wei HH, Ma MX et al. Lateral artificial synapses on hybrid perovskite platelets with modulated neuroplasticity. *Adv Funct Mater* **30**, 2005413 (2020).
16. Chen X, Chen BK, Jiang B, Gao TF, Shang G et al. Nanowires for UV–vis–IR optoelectronic synaptic devices. *Adv Funct Mater* **33**, 2208807 (2023).
17. Zhou K, Shang G, Hsu H, Han SH, Roy VAL et al. Emerging 2D metal oxides: from synthesis to device integration. *Adv Mater* **35**, 2207774 (2023).
18. Hong XT, Liu XQ, Liao L, Zou XM. Review on metal halide perovskite-based optoelectronic synapses. *Photon Res* **11**, 787–807 (2023).
19. Shrivastava S, Keong LB, Pratik S, Lin AS, Tseng TY. Fully photon controlled synaptic memristor for neuro-inspired computing. *Adv Electron Mater* **9**, 2201093 (2023).
20. Subramanian Periyal S, Jagadeeswararao M, Ng SE, John RA, Mathews N. Halide perovskite quantum dots photosensitized-amorphous oxide transistors for multimodal synapses. *Adv Mater Technol* **5**, 2000514 (2020).
21. Liu Y, Huang W, Wang XW, Liang RR, Wang J et al. A hybrid phototransistor neuromorphic synapse. *IEEE J Electron Dev Soc* **7**, 13–17 (2018).
22. Li Y, Shen GZ. Advances in optoelectronic artificial synapses. *Cell Rep Phys Sci* **3**, 101037 (2022).
23. Huang W, Hang PJ, Wang Y, Wang K, Han SH et al. Zero-power optoelectronic synaptic devices. *Nano Energy* **73**, 104790 (2020).
24. Hong S, Choi SH, Park J, Yoo H, Oh JY et al. Sensory adaptation and neuromorphic phototransistors based on CsPb$(Br_{1-x}I_x)_3$ perovskite and MoS_2 hybrid structure. *ACS Nano* **14**,

9796–9806 (2020).
25. Hao DD, Zhang JY, Dai SL, Zhang JH, Huang J. Perovskite/organic semiconductor-based photonic synaptic transistor for artificial visual system. *ACS Appl Mater Interfaces* **12**, 39487–39495 (2020).
26. Kumar M, Kim J, Wong CP. Transparent and flexible photonic artificial synapse with piezo-phototronic modulator: Versatile memory capability and higher order learning algorithm. *Nano Energy* **63**, 103843 (2019).
27. Zhai YB, Zhou Y, Yang XQ, Wang F, Ye WB et al. Near infrared neuromorphic computing via upconversion-mediated optogenetics. *Nano Energy* **67**, 104262 (2020).
28. Wang J, Shen H, Xia Y, Komarneni S. Light-activated room-temperature gas sensors based on metal oxide nanostructures: A review on recent advances. *Ceramics international* **47**, 7353–7368 (2021).
29. Benda J, Tabak J. Spike-frequency adaptation. In Jaeger D, Jung R. *Encyclopedia of Computational Neuroscience* 1–12 (Springer, New York, 2014); https://doi.org/10.1007/978-1-4614-7320-6_339-1.
30. Indiveri G, Linares-Barranco B, Hamilton TJ, van Schaik A, Etienne-Cummings R et al. Neuromorphic silicon neuron circuits. *Front Neurosci* **5**, 73 (2011).
31. Aamir SA, Müller P, Kiene G, Kriener L, Stradmann Y et al. A mixed-signal structured adex neuron for accelerated neuromorphic cores. *IEEE Trans Biomed Circ Syst* **12**, 1027–1037 (2018).
32. Hille B. Ionic channels in excitable membranes. Current problems and biophysical approaches. *Biophys J* **22**, 283–294 (1978).
33. Chizhov A, Rumyantseva M, Gaskov A. Light activation of nanocrystalline metal oxides for gas sensing: principles, achievements, challenges. *Nanomaterials* **11**, 892 (2021).
34. Gurlo A. Insights into the mechanism of gas sensor operation. In Carpenter MA, Mathur S, Kolmakov A. *Metal Oxide Nanomaterials for Chemical Sensors* 3–34 (Springer, New York, 2012); https://doi.org/10.1007/978-1-4614-5395-6_1.
35. Luo C, Kuner T, Kuner R. Synaptic plasticity in pathological pain. *Trends Neurosci* **37**, 343–355 (2014).
36. Tao J, Sarkar D, Kale S, Singh PK, Kapadia R. Engineering complex synaptic behaviors in a single device: emulating consolidation of short-term memory to long-term memory in artificial synapses via dielectric band engineering. *Nano Lett* **20**, 7793–7801 (2020).
37. Zhang JY, Sun TL, Zeng S, Hao DD, Yang B et al. Tailoring neuroplasticity in flexible perovskite QDs-based optoelectronic synaptic transistors by dual modes modulation. *Nano Energy* **95**, 106987 (2022).
38. Subin PS, Midhun PS, Antony A, Saji KJ, Jayaraj MK. Optoelectronic synaptic plasticity mimicked in ZnO-based artificial synapse for neuromorphic image sensing application. *Mater Today Commun* **33**, 104232 (2022).
39. Zhang JY, Dai SL, Zhao YW, Zhang JH, Huang J. Recent progress in photonic synapses for neuromorphic systems. *Adv Intell Syst* **2**, 1900136 (2020).
40. Tetzlaff C, Kolodziejski C, Timme M, Tsodyks M, Wörgötter F. Synaptic scaling enables dynamically distinct short- and long-term memory formation. *PLoS Comput Biol* **9**, e1003307 (2013).
41. Rosahl TW, Geppert M, Spitlane D, Herz J, Hammer RE et al. Short-term synaptic plasticity is altered in mice lacking synapsin I. *Cell* **75**, 661–670 (1993).
42. Benda J. Neural adaptation. *Curr Biol* **31**, R110–R116 (2021).
43. Glanzman DL. Habituation in *Aplysia*: the Cheshire cat of neurobiology. *Neurobiol Learn Mem* **92**, 147–154 (2009).
44. Gerstner W, Kistler WM, Naud R, Paninski L. *Neuronal Dynamics*: *From Single Neurons to Networks and Models of Cognition*. (Cambridge University Press, Cambridge, 2014).
45. Zuo F, Panda P, Kotiuga M, Li JR, Kang MG et al. Habituation based synaptic plasticity and organismic learning in a quantum perovskite. *Nat Commun* **8**, 240 (2017).
46. Janotti A, van de Walle CG. Native point defects in ZnO. *Phys Rev B* **76**, 165202 (2007).
47. Chizhov A, Kutukov P, Gulin A, Astafiev A, Rumyantseva M. Highly active nanocrystalline ZnO and its photo-oxidative properties towards acetone vapor. *Micromachines* **14**, 912 (2023).
48. Markram H, Toledo-Rodriguez M, Wang Y, Gupta A, Silberberg G et al. Interneurons of the neocortical inhibitory system. *Nat Rev Neurosci* **5**, 793–807 (2004).
49. Jolivet R, Lewis TJ, Gerstner W. Generalized integrate-and-fire models of neuronal activity approximate spike trains of a detailed model to a high degree of accuracy. *J Neurophysiol* **92**, 959–976 (2004).
50. Izhikevich EM. Simple model of spiking neurons. *IEEE Trans Neural Netw* **14**, 1569–1572 (2003).
51. Brette R, Gerstner W. Adaptive exponential integrate-and-fire model as an effective description of neuronal activity. *J Neurophysiol* **94**, 3637–3642 (2005).
52. Tabas A, Mihai G, Kiebel S, Trampel R, von Kriegstein K. Abstract rules drive adaptation in the subcortical sensory pathway. *eLife* **9**, e64501 (2020).
53. Maravall M, Alenda A, Bale MR, Petersen RS. Transformation of adaptation and gain rescaling along the whisker sensory pathway. *PLoS One* **8**, e82418 (2013).
54. Dhruv NT, Carandini M. Cascaded effects of spatial adaptation in the early visual system. *Neuron* **81**, 529–535 (2014).
55. Chizhov AS, Rumyantseva MM, Drozdov KA, Krylov IV, Batuk M et al. Photoresistive gas sensor based on nanocrystalline ZnO sensitized with colloidal perovskite $CsPbBr_3$ nanocrystals. *Sens Actuat B Chem* **329**, 129035 (2021).
56. Brunauer S, Emmett PH, Teller E. Adsorption of gases in multimolecular layers. *J Am Chem Soc* **60**, 309–319 (1938).

Acknowledgements

This work was supported by the Ministry of Science and Higher Education of the Russian Federation (Grant № 075-15-2020-801) and by Non-commercial Foundation for support of Science and Education «INTELLECT». We also acknowledge Mikhail Kik for the assistance in 3D schematic illustration.

Author contributions

IS Balashov: Conceptualization, Methodology, Writing - Original Draft preparation
AA Chezhegov: Investigation, Visualization, Data Curation
AS Chizhov: Investigation, Resources
AA Grunin: Conceptualization, Validation, Writing - Review & Editing
KV Anokhin: Conceptualization, Writing - Review & Editing
AA Fedyanin: Supervision, Writing - Review & Editing

Competing interests

The authors declare no competing financial interests.